11th World Congress on Structural and Multidisciplinary Optimisation
07th -12th, June 2015, Sydney Australia

Simultaneous Optimization of Initial Blank Shape and Blank Holder Force Trajectory for Square Cup Deep Drawing Using Sequential Approximate Optimization

Satoshi Kitayama[1], Marina Saikyo[2] , Kiichiro Kawamoto[3], Ken Yamamichi[4]

[1] Kanazawa University, Kanazawa, Japan, kitayama-s@se.kanazawa-u.ac.jp
[2] Graduate School of Natural Science & Technology, Kanazawa University, Kanazawa, Japan, saikyo@stu.kanazawa-u.ac.jp
[3]Komatsu Industry Corp., Komatsu, Japan, kiichirou_kawamoto@komatsu.co.jp
[4]Komatsu Industry Corp., Komatsu, Japan, ken_yamamichi@komatsu.co.jp

1. Abstract
Optimal blank shape minimizing earing in deep drawing has a direct influence on material saving as well as product quality. This paper proposes a method for determining the optimal blank shape design in square cup deep drawing using sequential approximate optimization (SAO) with a radial basis function (RBF) network. The earing is minimized under tearing and wrinkling constraints with a variable blank holder force (VBHF), which varies through the punch stroke. Through numerical and experimental results, the validity of the proposed approach is examined.
2. Keywords: Deep Drawing Blank Shape Design, Variable Blank Holder Force, Sequential Approximate Optimization

3. Introduction

Sheet metal forming processes involve a complicated deformation that is affected by process parameters such as material properties, blank holder force (BHF), die geometry, blank shape, friction, and lubrication condition. Among these, the blank shape has a direct influence on the product quality. The desired product cannot be obtained with a small initial blank shape, while a large initial blank shape produces a large flange part that is trimmed off as waste. Furthermore, a small BHF can lead to wrinkling while a large BHF results in tearing. Thus, it is important to find a suitable blank shape with an optimal BHF for the material saving and product quality. A number of different approaches have been proposed to determine the optimal blank shape in deep drawing, and these are mainly classified into two categories: the use of a closed-loop type algorithm, or those based on the response surface method (RSM).
Sheet forming simulation is currently so numerically intensive that the use of RSM is a valid option. Hino et al. used the RSM for obtaining the optimal blank shape in deep drawing [1], in which earing, as defined by the amount of trimmed material, was minimized under two design constraints. Naceur et al. used a moving least square approximation to determine the optimal blank shape [2], for which the risk of tearing/wrinkling was approximated using a quadratic polynomial, and 7 control points (nodes of the blank) were taken as the design variables.
This paper proposes a method for determining the optimal blank shape with the VBHF in deep drawing. The objective is to find out the optimal blank shape minimizing the earing under tearing/wrinkling constraints with the VBHF approach. In this paper, two objective functions are developed to evaluate the earing. The tearing/wrinkling is evaluated using the forming limit diagram (FLD) and are regarded as the design constraints. In order to identify a set of paret-optimal solutions with a small number of simulation runs, a sequential approximate optimization using the RBF network has been adopted. The validity of the proposed approach is examined through the experiment using a servo press.

4. Blank Shape Optimization with Variable Blank Holder Force

4.1. Finite element analysis model

The FEA model used in this paper is shown in Fig.1, in which the blank holder force is applied in the positive *z*-direction. The counter punch and die drop to the negative *z*-direction with a total stroke of 62 mm. The element type and the number of finite elements are shown in Table 1. The friction coefficient μ of the interfaces (blank/blank holder, blank/punch, blank/die, and blank/counter punch) is set to 0.10. Considering the symmetry, one-quarter model is used for the numerical simulation as shown in Fig.1. An initial blank size of 92.5 mm $\times$ 92.5 mm is actually used. A Belyschko-Tsay shell element with seven integration points along the thickness direction is used for the shell mesh of the blank. The penalty coefficient for contact (blank/blank holder, blank/punch, blank/die, and blank/counter punch) is set to 0.10. The element types and the number of finite elements are listed in Table 1. In addition, Steel Plate Formability Cold (SPFC) 440 is selected as the test material. The material properties are listed in Table 2.

The quarter-model deformation of the initial blank is shown in Fig. 2, in which the dashed line represents the target (trimmed) contour and the area above this contour is defined as earing. As shown in Fig. 2, the earing in this square cup deep drawing is generated in the *x*-*y* plane. Ideally, the target contour should be set to the exact shape of the product denoted by the bold line. However, it is very difficult to set the exact shape as the ideal target contour in this deep drawing. The tolerance of 5 mm from the exact shape is then considered and is set as the target contour.

Table 1 Element type and number of finite elements

	Element type	Number of finite elements
Counter punch	Rigid	120
Die	Rigid	924
Blank	Shell (Belytschko-Tsay)	2116
Blank holder	Rigid	432
Punch	Rigid	962

Table 2 Material properties of SPFC440

Density: ρ [kg/mm^3]	7.84×10^{-6}
Young's Modulus: E [MPa]	2.06×10^{5}
Poisson's Ratio: ν	0.3
Yield Stress: σ_Y [MPa]	353
Tensile Strength: σ_T [MPa]	479
Normal Anisotropy Coefficient: r	0.98
Strain Hardening Coefficient: n	0.189

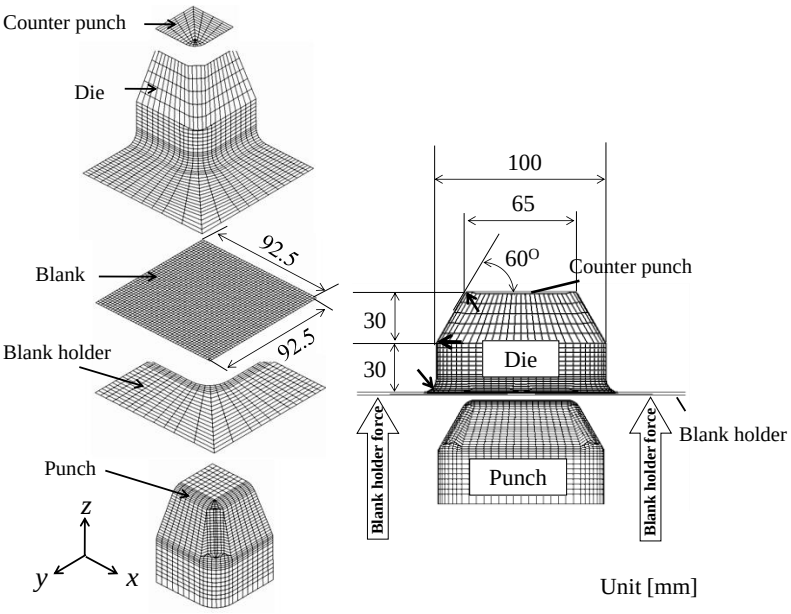

Fig.1 Finite element analysis model

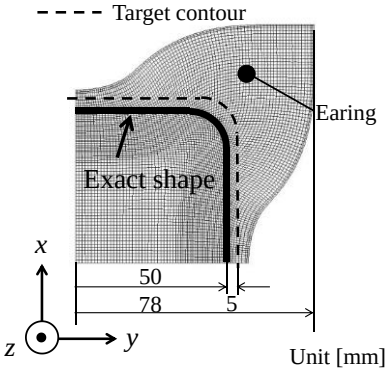

Fig.2 Deformation of initial blank (quarter model)

4.2. Design Variables

The blank shape is determined using the four design variables shown in Fig.3, where one-quarter model of the formed product is depicted. The three nodes denoted by black squares are taken as the design variables for determining the blank shape. Nodes 1 and 3 move along the vertical and 45 degree line, respectively, while the movement of Node 2 depends on x_4. These nodes are connected by straight line as shown in Fig. 3, and the initial blank shape is then determined. VBHF is also taken into consideration to control the material flow into the die. For the VBHF, total stroke L_{max} is partitioned into n sub-stroke steps and the BHF of each sub-stroke is taken as the design variables. An illustrative example of these design variables is shown in Fig.4, where it should be noted that the design variable for VBHF starts from x_5.

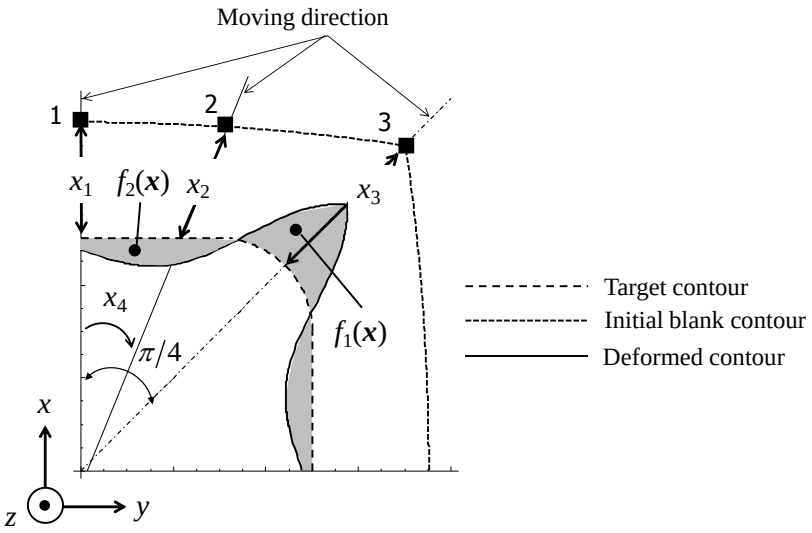

Fig.3 Illustrative example for evaluating earing and design variables for blank shape

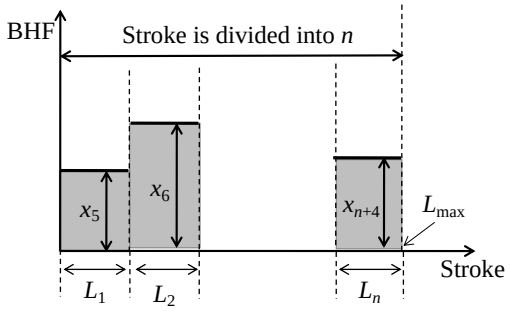

Fig.4 Design variables for variable blank holder force

4.3. Objective functions

Let us explain how to evaluate the earing with Fig.3, in which the dashed line represents the target (trimmed) contour. First, the area above the target contour is evaluated as the first objective function $f_1(\boldsymbol{x})$, as shown in Fig.3. Unfortunately, in this method, the area below the target contour cannot also be evaluated. Consequently, this area below the target contour is evaluated as the second objective function $f_2(\boldsymbol{x})$. As $f_1(\boldsymbol{x})$ will be large with a large blank shape, while $f_2(\boldsymbol{x})$ will be large with a small blank shape, a trade-off between these objectives can thus be observed.

4.4. Constraints

The forming limit diagram (FLD) is used to evaluate the tearing and wrinkling. In order to evaluate the degree of tearing and wrinkling, the strains in the formed element are analyzed and compared against the forming limit curve (FLC, as shown in Fig.5). The following FLC was defined in the principal plane of logarithmic strains proposed by Hillman and Kubli [5].

$$\varepsilon_1 = \varphi_T(\varepsilon_2) \quad \varepsilon_1 = \varphi_W(\varepsilon_2) \tag{1}$$

where φ_T is the FLC that controls tearing, and φ_W is the FLC that controls wrinkling. The following safety FLC

is defined:

$$\left.\begin{aligned}\theta_T(\varepsilon_2) &= (1-s)\varphi_T(\varepsilon_2)\\ \theta_W(\varepsilon_2) &= (1+s)\varphi_W(\varepsilon_2)\end{aligned}\right\} \tag{2}$$

where *s* represents the safety tolerance, and is defined by the engineers (in this paper, *s* is set to 0.2). If an element comes to or lies above FLC, it is expected that a risk of tearing can be observed. Similarly, a risk of wrinkling can be assumed if an element lies in the wrinkling region. The risk of both wrinkling and tearing were evaluated as follows:
For tearing:

$$g_1(\boldsymbol{x}) = \left(\sum_{j=1}^{nelm} T_j\right)^{1/p} \tag{3}$$

where

$$\begin{aligned} T_j &= (\varepsilon_1^j - \theta_T(\varepsilon_2^j))^p \quad \varepsilon_1^j > \theta_T(\varepsilon_2^j)\\ T_j &= 0 \qquad\qquad otherwise\end{aligned} \tag{4}$$

For wrinkling:

$$g_2(\boldsymbol{x}) = \left(\sum_{j=1}^{nelm} W_j\right)^{1/p} \tag{5}$$

where

$$\begin{aligned} W_j &= (\theta_W(\varepsilon_2^j) - \varepsilon_1^j)^p \quad \varepsilon_1^j < \theta_W(\varepsilon_2^j)\\ W_j &= 0 \qquad\qquad otherwise\end{aligned} \tag{6}$$

p is set to 4, and *nelm* represents the number of finite elements of the blank.

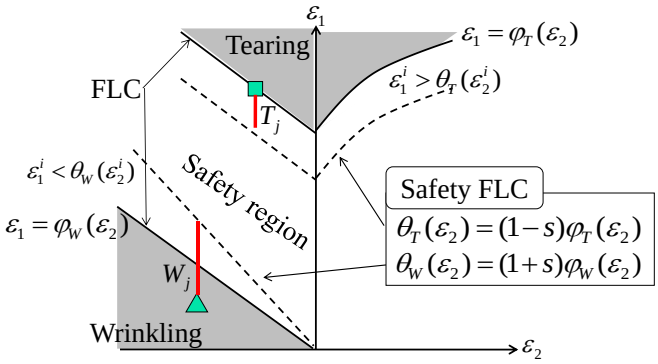

Fig.5 Forming limit diagram for evaluating tearing and wrinkling

5. Flow of Sequential Approximate Optimizatoin

The flow can be summarized as follows:
(STEP1) Initial sampling points are generated by the LHD.
(STEP2) Numerical simulation is carried out, in which objective functions ($f_1(\boldsymbol{x})$ and $f_2(\boldsymbol{x})$) and constraints ($g_1(\boldsymbol{x})$ and $g_2(\boldsymbol{x})$) are numerically evaluated at all sampling points.
(STEP3) All functions are approximated by the RBF network; wherein the approximated objective functions are denoted as $\tilde{f}_i(\boldsymbol{x})$ ($i = 1,2,\cdots,K$), and the approximated constraint functions are denoted as $\tilde{g}_j(\boldsymbol{x})$ ($j = 1,2,\cdots,m$).

(STEP4) A pareto-optimal solution for the response surface is found using the weighted *lp* norm method:

$$\left.\begin{aligned}&\left[\sum_{i=1}^{K}\left(\alpha_i \tilde{f}_i(\boldsymbol{x})\right)^p\right]^{1/p} \rightarrow \min\\ &\tilde{g}_j(\boldsymbol{x}) \le 0 \quad j = 1,2,\cdots,m\end{aligned}\right\} \tag{7}$$

where α_i ($i = 1,2,\cdots,K$) represents the weight of the *i*-th objective function, and *p* is the parameter (set to 4 in this paper). In order to obtain a set of pareto-optimal solutions, various weights are assigned.
(STEP5) The density function is constructed and minimized, and the optimal solution of the density function is added as a new sampling point [4]. This step is repeated till a terminal criterion is satisfied.

(STEP6) If terminal criterion is satisfied, the SAO algorithm will be terminated. Otherwise, return to STEP 2.

5. Numerical and Experimental Results

Numerical simulation was carried out to obtain the optimal blank shape and VBHF. For the VBHF, the total stroke was divided into 3 (L_1, L_2, and L_3). Then, the total number of design variables is 7. The lower and upper bounds of the design variables are defined as follows:

$$\left.\begin{array}{l} 38 \le x_1 \le 42.5[mm] \quad 33 \le x_2 \le 40[mm] \quad 23 \le x_3 \le 62[mm] \\ \pi/12 \le x_4 \le \pi/6[rad] \\ 20 \le x_5 \le 120[kN] \quad for \quad 0 \le L_1 \le 20[mm] \\ 20 \le x_6 \le 120[kN] \quad for \quad 20 \le L_2 \le 40[mm] \\ 20 \le x_7 \le 120[kN] \quad for \quad 40 \le L_3 \le 62[mm] \end{array}\right\} \tag{7}$$

Fifteen initial sampling points are first generated with the LHD, and the pareto-frontier is identified. The error in the pareto-optimal solutions is adopted as the terminal criterion, which is set to 5.0 %. Various weights are assigned to the each objective function, and a total of 56 sampling points (simulation runs) are required to identify the pareto-frontier. All feasible sampling points in the objective space are shown in Fig.6. It can be seen that the pareto-frontier is disconnected. Furthermore, we can also see that the optimal blank shape and the deformed shape are not qualitatively different, but the same is not true in the case of the optimal VBHF.

At point A, the initial BHF is low but gradually increases. This implies that the material readily flows into the die with the low BHF, but becomes hardened as the BHF increases. On the other hand, at point B, the material is hardened at the initial stage by the high BHF; with the lower BHF needing to be applied during the middle stage in order to prevent tearing. Finally, the material is again hardened by the high BHF at the final stage.

Based on the numerical results, the experiments using a servo press (H1F200, Komatsu Industry Corp.) are carried out. The photos of punch and blank holder are shown in Fig. 7. Points A and B shown in Fig.6 is used for the experiments. An expert commented that the blank holder will be injured if the optimal blank obtained the numerical result is directly used in the experiment. Based on his suggestion, the blank shape considering the tolerance of 5 mm is used, which is shown in Fig. 7. The VBHF trajectory and the product through the experiments are shown in Figs. 8 and 9, respectively. It is found from the experimental results that no tearing/wrinkling can be observed. The validity of the proposed approach is confirmed through the numerical and experimental results.

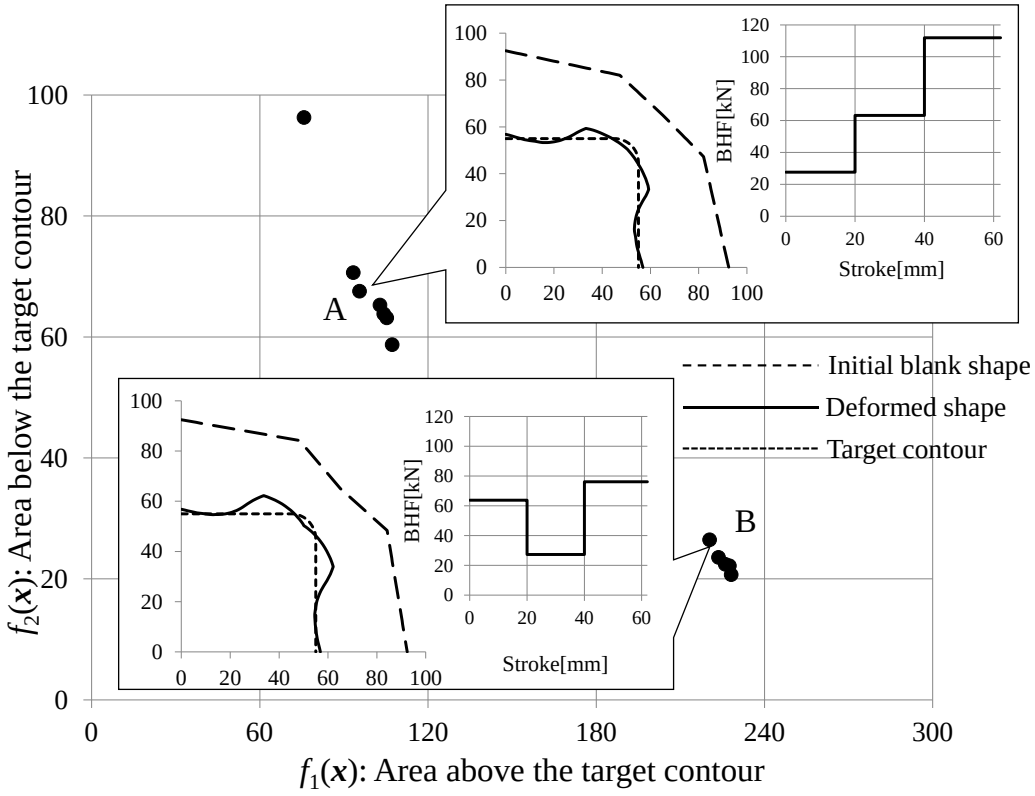

Fig.6 Pareto-frontier with an optimal blank shape and VBHF

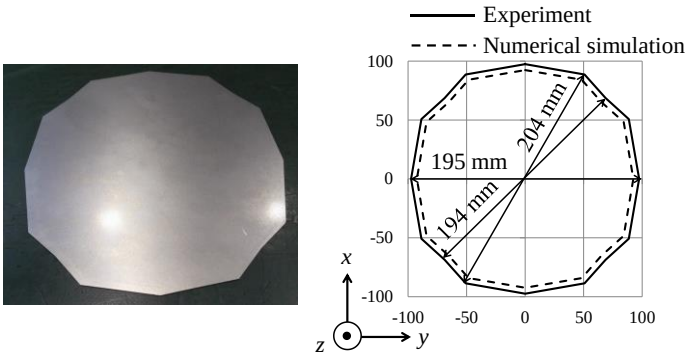

Fig. 7 Blank shape used in the experiment

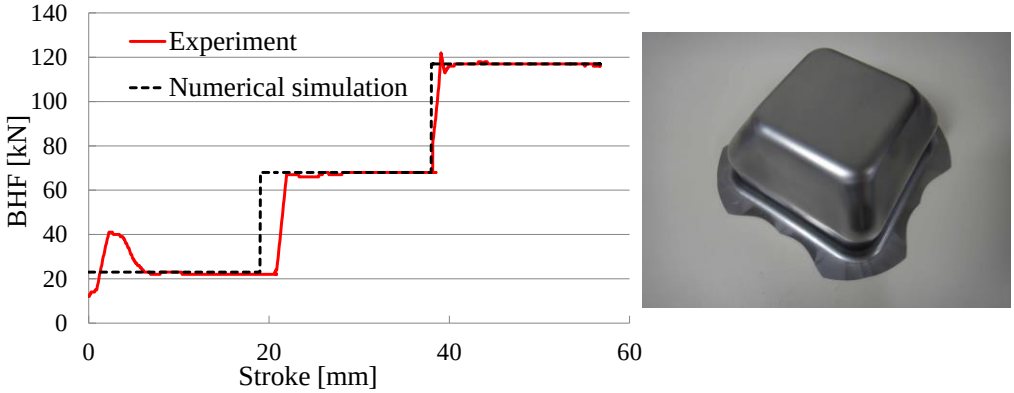

Fig. 8 VBHF trajectory and product at point A

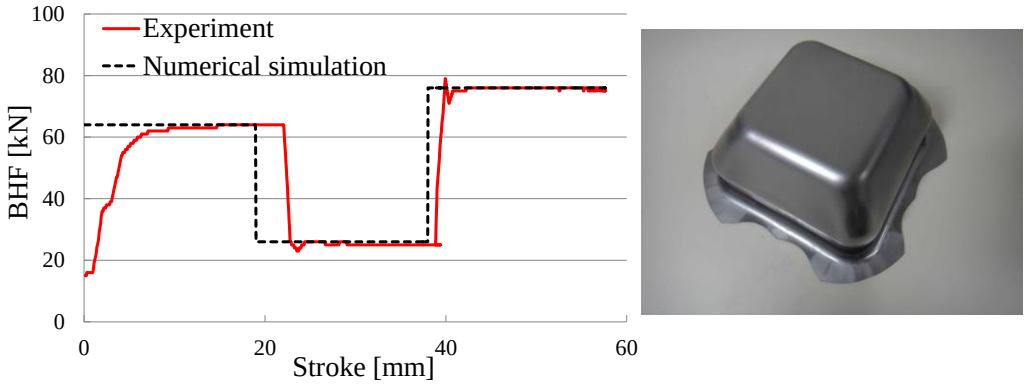

Fig. 9 VBHF trajectory and product at point B

6. Concluding Remarks

This paper proposes a method to determine the optimal blank shape minimizing the earing and the optimal VBHF trajectory. The numerical result indicates that there are two kinds of VBHF trajectories for the successful sheet forming whereas the optimal blank is qualitatively same. Based on the numerical results, the experiments using servo press is carried out. No tearing/wrinkling can be observed through the experiments, and the validity of the proposed approach is then confirmed.

References

[1] Hino, R., Yoshida, F., Toropov, V.V., (2006), Optimum blank design for sheet metal forming based on the interaction of high- and low-fidelity FE models, *Archive of Applied Mechanics*, 75(10): 679-691.

[2] Naceur, H., Ben-Elechi, S., Batoz, J.L., Knopf-Lenoir, C., (2008), Response surface methodology for the rapid design of aluminum sheet metal forming parameters, *Materials and Design*, 29: 781-790.

[3] Hillmann, M., Kubli, W., (1999), Optimization of sheet metal forming processes using simulation programs, in : *Numisheet '99*, Beasnc, France, 1: 287-292.

[4] Kitayama, S., Arakawa, M., Yamazaki, K., (2011), Sequential approximate optimization using radial basis function network for engineering optimization, *Optimization and Engineering*, 12(4): 535-557.